Theoretical and Experimental Studies of the Bell-Jar-Top Inductively Coupled Plasma

Han-Ming Wu, Ben W. Yu, Anantha Krishnan, Ming Li, Yun Yang, Jia-Ping Yan, and Ding-Pu Yuan

***Abstract*—The present paper describes a systematic study of argon plasmas in a bell-jar inductively coupled plasma (ICP) source over the range of pressure 5–20 mtorr and power input 0.2–0.5 kW. Experimental measurements as well as results of numerical simulations are presented. The models used in the study include the well-known global balance model (or the global model) as well as a detailed two-dimensional (2-D) fluid model of the system. The global model is able to provide reasonably accurate values for the global electron temperature and plasma density. The 2-D model provides spatial distributions of various plasma parameters that make it possible to compare with data measured in the experiments. The experimental measurements were obtained using a tuned Langmuir double-probe technique to reduce the RF interference and obtain the light versus current (I–V) characteristics of the probe. Time-averaged electron temperature and plasma density were measured for various combinations of pressure and applied RF power. The predictions of the 2-D model were found to be in good qualitative agreement with measured data. It was found that the electron temperature distribution T_e was more or less uniform in the chamber. It was also seen that the electron temperature depends primarily on pressure, but is almost independent of the power input, except in the very low-pressure regime. The plasma density goes up almost linearly with the power input.**

***Index Terms*—Experimental diagnosis, ICP, 2-D modeling.**

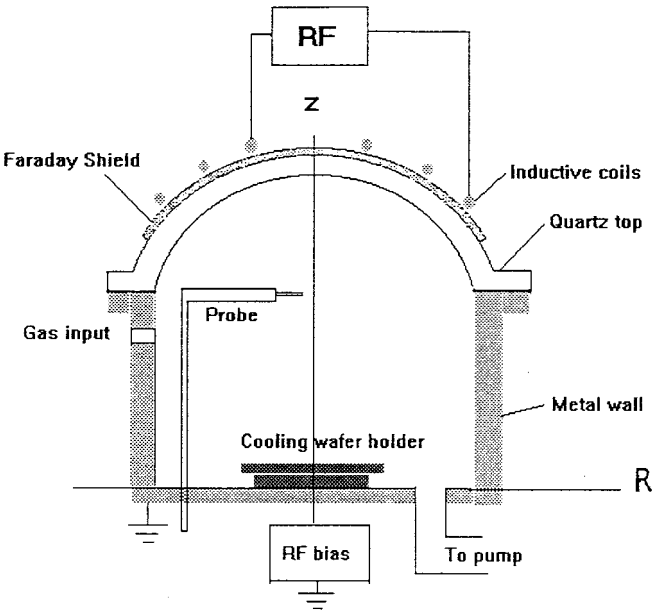

Fig. 1. Schematic of the bell-jar-top ICP apparatus.

I. Introduction

THE limitations of radio frequency (RF) diodes have led to the development of new plasma sources, such as the electron cyclotron resonance (ECR) plasma sources and the inductively coupled plasma (ICP) sources. These sources operate at low-pressure and high-plasma density. Plasma densities in these enhanced plasma sources can reach $10^{11-12}/\text{cm}^3$, while the neutral pressures are in the range of 1–50 mtorr [1]–[3]. As a new kind of plasma source, the ICP has appealed to many scientists due to its structural simplicity. Accompanying this surge of studies on the new generation plasma source has been an effort to understand the plasma behavior in ICP [4]–[8] systems.

Low-pressure, high-density plasma sources have been employed for etch and deposition processings for a few years. Since then, a considerable amount of research has gone into the analysis of ECR and ICP systems [5]–[9]. Computer modeling has been used extensively to gain insight into low-pressure discharge behavior, particularly for enhanced plasma sources. Most modeling studies have made use of either the fluid model or the particle Monte Carlo method, or the hybrid models [10]–[12]. It has been found that the fluid models are able to resolve much of the relevant physics with reasonable accuracy within a tolerable computational cost. The Monte Carlo technique is a valuable tool to verify the accuracy of the fluid model, as well as any *a priori* assumptions about the particle distribution functions. Recently, nonlocal electron kinetics has been studied to revise the Boltzmann equation [16], [17].

The modeling work described in this paper includes results from the global model as well the two-dimensional (2-D) fluid model. A brief comparison of the results from the two models is performed. Langmuir probe measurements are a powerful and experimentally simple means of determining key internal discharge parameters, such as plasma density, electron temperature, and electron energy distribution function (EEDF) [18]. In a dc discharge, the plasma potential is invariant with time, whereas in an RF discharge, the plasma potential fluctuates with time. Although the Faraday shield is still employed, there is still some capacitive component with

Manuscript received December 2, 1996; revised March 10, 1997. The work was supported in part by the Presidential Foundation of the Chinese Academy of Sciences. This development and application of the 2-D fluid model was done by DARPA under Contract DAAH01-95-C-R146.

H.-M. Wu, B. W. Yu, and A. Krishnan are with the CFD Research Corporation, Huntsville, AL 35805 USA (e-mail: hmw@cfdrc.com).

M. Li, Y. Yang, and J.-P. Yan are with the Institute of Mechanics, Academia Sinica, Beijing, China.

D.-P. Yuan is with the Institute of Physics, Academia Sinica, Beijing, China.

Publisher Item Identifier S 0093-3813(97)05537-9.

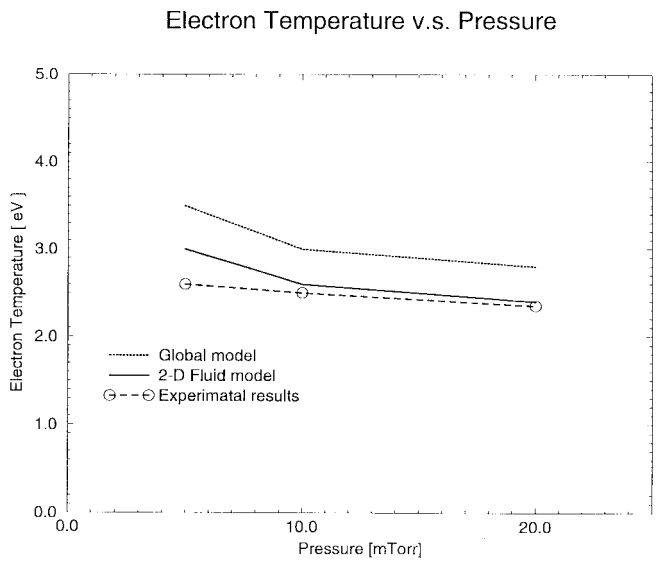

Fig. 2. Global model, 2-D fluid model, and diagnostic results, respectively. Electron temperature T_e versus neutral pressure p; power input $P_{\rm abs} = 200$ W.

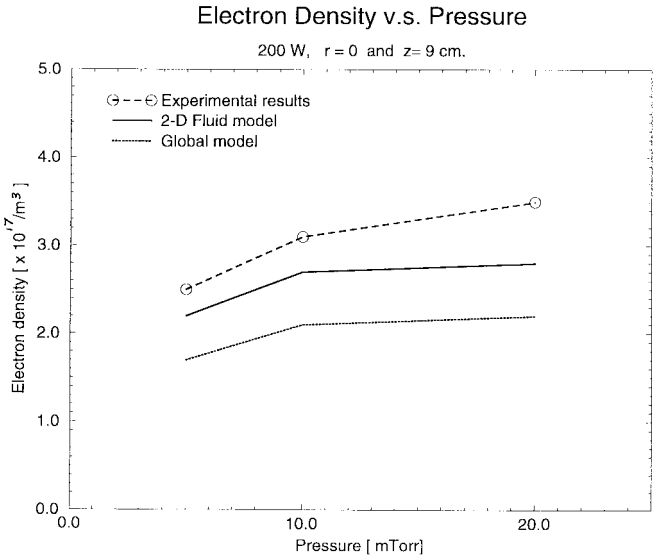

Fig. 3. Global model, 2-D fluid model, and diagnostic results, respectively. Electron density n_e versus neutral pressure p_n, power input $P_{\rm abs} = 200$ W.

the ICP, and the potential varies with time. The RF voltage from plasma would shift the apparent floating potential to a more negative value and distort the probe characteristic. The electron temperature obtained from the distorted characteristic usually exceeds the true value, while the electron density is underestimated [13], [15]. Using a tuned Langmuir probe minimizes the RF-induced distortion of the probe characteristic in the measurement of the electron temperature and plasma density.

Geometry Descriptions: The ICP reactor described in this paper employs a new design in which a bell-jar quartz top is used. Especially for a large-area chamber, the larger thickness and larger mass of quartz lead to longer heating time. It has the potential to reduce the thickness of the dielectric layer and the cost. This is because no vacuum chamber (low pressure) on the top is required, although the thickness of quartz is only 0.5 cm. In addition, a uniform plasma profile can be achieved by adjusting the wafer stage position. The uniformity in the planar coil ICP is primarily determined by the inductive coil geometry [5], [9]. The geometry of the ICP chamber is shown in Fig. 1. The bottom chamber is made of stainless steel with radius $R = 12$ cm and height $L = 8$ cm, respectively. The top of the bell-jar cover, with radius of curvature 13 cm, is insulated, whereas the bottom is grounded. The dome cover is made of quartz with 0.5-cm thickness.

II. Theoretical Modeling

This section describes the formulation and governing equations for the global model and the 2-D fluid model.

A. Global Model

A global model developed by Lieberman and Gottscho has proved to be effective in estimating plasma parameters in an enhanced plasma source [1], [4], [5]. With this method, it is possible to estimate certain plasma parameters as well as a qualitative description of their dependence on operating conditions. Although the global model has been previously discussed in detail for the bell-jar ICP, it is rederived here for the convenience of the reader [8].

Previous comparisons have shown that the global model can give a relatively accurate estimation with minimum computational cost unless the spatial distributions of plasma parameters are required [5], [12]. The relevant second-order rate constants, such as electron–neutral ionization K_{iz}, excitation K_{ex}, metastable K_{me}, and elastic scattering K_{el} are the same as in [5]. The expression for the rate coefficients of the inelastic processes all have the same form

$$K_i(T_e) = \sigma_i \overline{v}_e \exp\left(-\frac{E_i}{kT_e}\right) \tag{1}$$

where σ_i and $\overline{v}_e$ are the scattering cross section and mean electron thermal speed $\sqrt{8kT_e/\pi m_e}$, and the subscript "i" denotes the ith inelastic scattering.

1) Global Particle Balance: On the basis of the conservation law, the ion–electron pairs are created in the bulk plasma by electron-neutral ionization and are lost by flow to the walls. Ions are lost from the discharge after being accelerated to the Bohm velocity $u_B = \sqrt{kT_e/m_i}$ at the sheath edge, where m_i is ion mass. If the ionization rate K_{iz} is uniform in the space, then

$$K_{iz} N n V = \Gamma = \Gamma_b + \Gamma_s + \Gamma_t \tag{2}$$

where N, n, V, Γ_b, Γ_s, and Γ_t are the neutral gas density, the plasma density, chamber volume, and the ion fluxes on the bottom wall, sidewall, and top dome wall, respectively. These

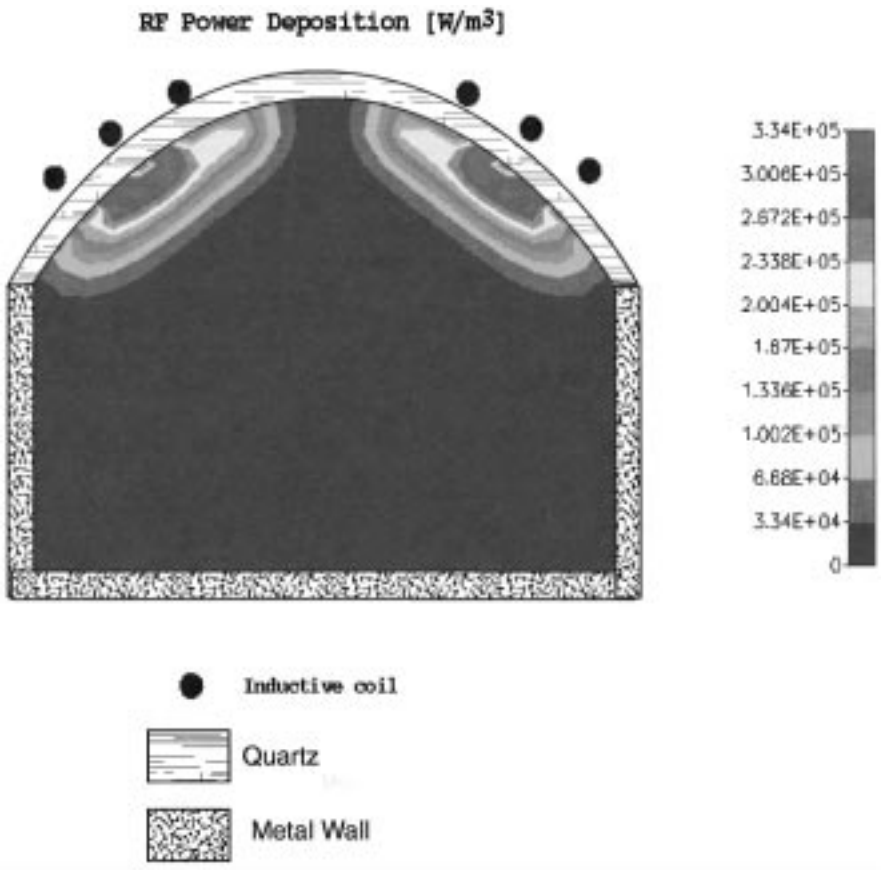

Fig. 4. Fluid model simulation result and spatial profile of the power deposition, where $P_{\rm abs} = 200$ W, nad $p_n = 10$ mtorr.

fluxes can be expressed as

$$\begin{aligned}\Gamma_b &= \pi R^2 h_L n u_B \\ \Gamma_s &= 2\pi R L h_R n u_B \\ \Gamma_t &= \int_s n u_B (h_L \cos\theta + h_R \sin\theta)\, ds \\ &= 2\pi R^2 n u_B \int_s (0.5 h_L \sin 2\theta + h_R \sin^2\theta)\, d\theta \\ &= \pi R^2 n u_B (a h_L + 2 b h_R)\end{aligned}$$

where $a = \int_s \sin 2\theta\, d\theta = 0.85$, $b = \int_s \sin^2\theta\, d\theta = 0.41$, and the integrate domain $s \in [0, 1.78]$ is the top spherical surface

$$h_L = 0.83\left(3 + \frac{0.5L}{\lambda_i}\right)^{-1/2}$$
$$h_R = 0.8\left(4 + \frac{R}{\lambda_i}\right)^{-1/2}$$

where

$$\lambda_i = \frac{1}{\sigma N}$$

is the ion–neutral mean–free path. σ and N are the ion–neutral momentum transfer cross section and neutral density, respectively.

2) Electron Temperature T_e: Conventionally, (2) is written as

$$\frac{K_{iz}(T_e)}{u_B} = \frac{\Gamma}{u_B N n V} = \frac{1}{N d_{\rm eff}} \tag{3}$$

where $d_{\rm eff} = V/\pi[h_L R^2(1+a) + 2h_R R(L + Rb)]$ is the so-called effective plasma size. Because new ion–electron creation is primarily from ionization, the other processes do not directly affect the plasma density. Equation (3) implies that the electron temperature is independent of the power input. Therefore, it can be concluded that the electron temperature is not determined by the electron energy balance but rather by the ion-neutral mean free path λ_i.

3) Plasma Density n and Ion Current Density on Wafer J_b: n depends primarily on the total power balance. For argon discharge, it is useful to define ε_c as the collisional energy lost per electron–ion pair created

$$\varepsilon_c = \varepsilon_{\rm ion} + \frac{K_{ex}+K_{me}\varepsilon_{me} + K_{eL}\varepsilon_{eL}}{K_{\rm ion}} \tag{4}$$

where $\varepsilon_{\rm ion} = 15.75$ eV, $\varepsilon_{ex} = 14.1$ eV, $\varepsilon_{me} = 12$ eV, and $\varepsilon_{el} = 3m_e kT_e/m_i$ are the energy lost per electron as a result of ionization, electronic excitation, metastable creation, and elastic collisions, respectively. The mean kinetic energy lost per electron recombination at the wall is $2kT_e$, and the kinetic energy per ion flowing out the plasma bulk is about $5.2kT_e$. Therefore, the total energy lost per electron–ion pair in the

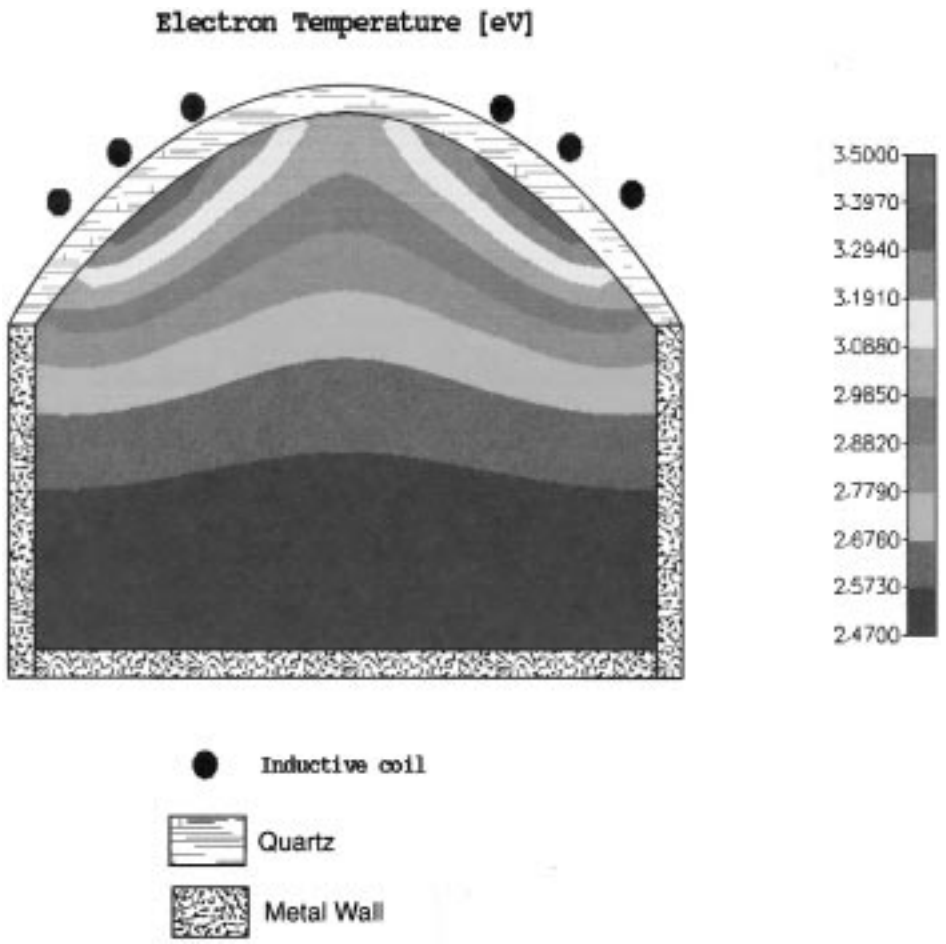

Fig. 5. Fluid model simulation result and spatial profile of the electron temperature T_e, where $P_{\rm abs} = 200$ W, and $p_n = 10$ mtorr.

system can be expressed as

$$\varepsilon_L = \varepsilon_c + 5.2kT_e + 2kT_e = \varepsilon_c + 7.2kT_e. \tag{5}$$

The overall global energy balance for the ICP can be written in terms of ε_L as

$$P_{\rm abs} = eu_B n_s A_{\rm eff} \varepsilon_L \tag{6}$$

where

$$n_s A_{\rm eff} = \pi n R^2 h_L + 2R\pi n L h_R + \int_s n(h_L \cos\theta + h_R \sin\theta)\, d\theta. \tag{7}$$

$P_{\rm abs}$ is the power absorbed in the plasma, and n_s is the plasma density at the presheath. This equation can be solved for the plasma density:

$$n = P_{\rm abs} \Big/ \left\{ eu_B \varepsilon_L \left[\pi R^2 h_L + 2R\pi L h_R + \int_s (h_L \cos\theta + h_R \sin\theta)\, d\theta \right] \right\}.$$

B. 2-D Fluid Model

1) Fluid Equations: The basic assumptions of the model are as follows.

1) The effects of the neutral gas flow are not considered at this time.
2) The ion temperature is the same as that of the neutral gas.
3) The inductive coils are simplified as three coaxial circular coils.
4) Electron distribution is assumed to be Maxwellian.
5) Neutral density and temperature are assumed to be uniform in the chamber.

The neutral argon gas pressure is treated as a parameter in this study and is varied from 5 to 20 mtorr.

The discharge model consists of a set of an electron continuity equation, an electron energy equation, and Maxwell equations for power deposition. In the current model, the bell-jar top is modeled by means of stepped grids. The equations are solved by assuming initial 2-D profiles for density and temperature, and stepping in time until a steady-state condition is reached. The time-averaged equations for electrons and ions are

$$\nabla \cdot \boldsymbol{J}_e = R_i \tag{8}$$

$$\nabla \cdot \boldsymbol{J}_i = R_i \tag{9}$$

$$\nabla \cdot \boldsymbol{Q}_e = q_j - \Sigma_k R_k \varepsilon_k e \tag{10}$$

where the electron flux $\boldsymbol{J}_e$, ion flux $\boldsymbol{J}_i$, and electron energy

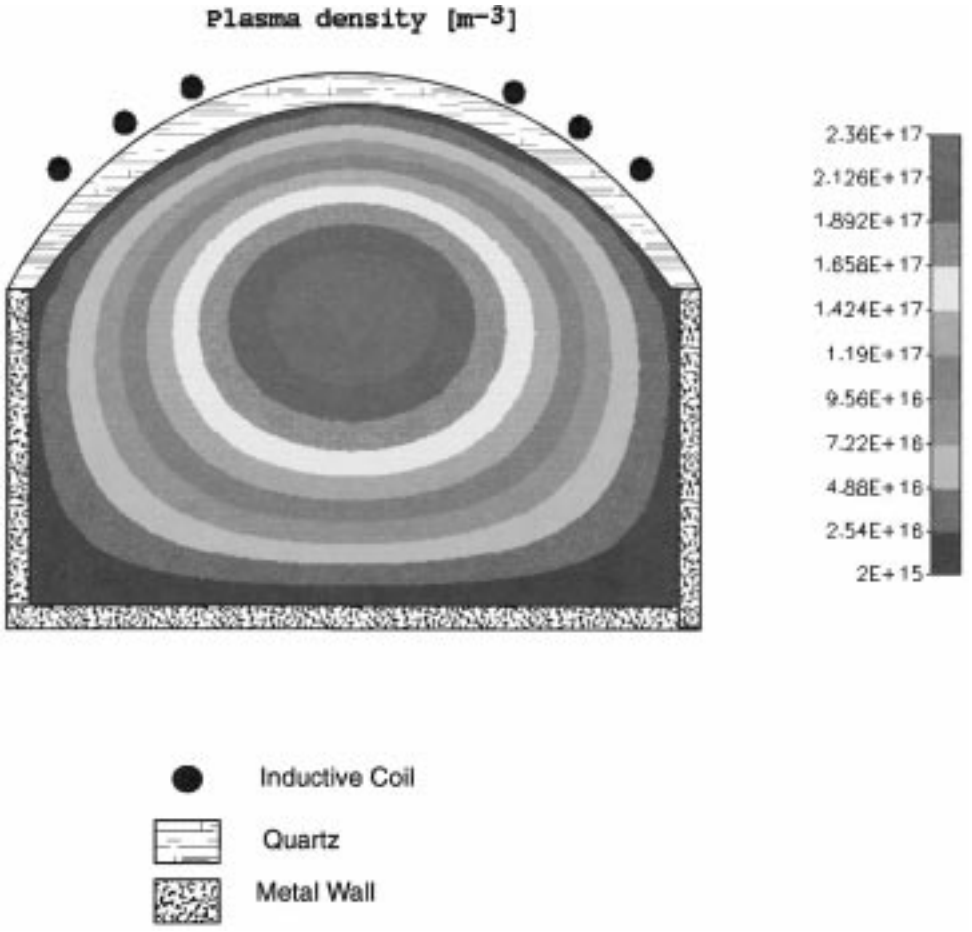

Fig. 6. Fluid model simulation result and spatial profile of the electron density n_e, where $P_{\rm abs} = 200$ W, and $p_n = 10$ mtorr.

flux $\boldsymbol{Q}_e$ are

$$\boldsymbol{J}_e = -\mu_e n_e \boldsymbol{E}_s - \left(\frac{k}{m_e \nu_{en}}\right)\nabla(n_e T_e)$$
$$\boldsymbol{J}_i = -\mu_i n_i \boldsymbol{E}_s - \left(\frac{2k}{m_i \nu_{iN}}\right)\nabla(n_i T_i)$$
$$\boldsymbol{Q}_e = 2.5(kT_e \boldsymbol{J}_e) - 2.5\left(\frac{k^2}{m_e \nu_{eN}}\right) n_e T_e \nabla T_e$$
$$\mu_e = \frac{e}{m_e \nu_{eN}}$$
$$\mu_i = \frac{2e}{m_i \nu_{iN}}$$
$$q_j = \frac{1}{T}\int_T \sigma_c E^2\, dt$$

where q_j is ohmic heating, $\boldsymbol{E}_s = -\nabla\phi$ is the plasma static electric field, μ_e and μ_i are the mobilities of the electron and ion, respectively, and

$$\sigma_c = \frac{n_e e^2}{m_e \nu_{eN}\left[1 + \left(\frac{\omega}{\nu_{eN}}\right)^2\right]}$$

is the electric conductivity. ν_{eN} and ω are the electron-neutral collision frequency and the RF frequency, respectively.

The total input power can be written as

$$P_{\rm abs} = 2\pi \iint q_j r\, dr\, dz.$$

The collision rate R_k can be expressed as $R_k = K_k n_e N$, where the subscript $k = iz$, ex, me, and el, respectively. In plasma bulk, the above set of fluid equations is closed with an ambipolar assumption.

The boundary conditions are the same as in our previous work [8], that is

$$n_e = \phi = \boldsymbol{n} \cdot \nabla T_e = 0$$

on the metallic wall ($\boldsymbol{n}$ is a normal unit vector to the wall) and

$$\frac{\partial n_e}{\partial r} = \frac{\partial n_i}{\partial r} = \frac{\partial \phi}{\partial r} = \frac{\partial T_e}{\partial r} = 0 \qquad (11)$$

on the axis.

2) Electromagnetic Equations: The net field consists of both inductive and plasma static fields, i.e., $E = E_I + \boldsymbol{E}_s$. Because of the axial symmetric assumption, the inductive electric field which has only azimuthal component is written as

$$E_I = E_1 \cos \omega t + E_2 \sin \omega t.$$

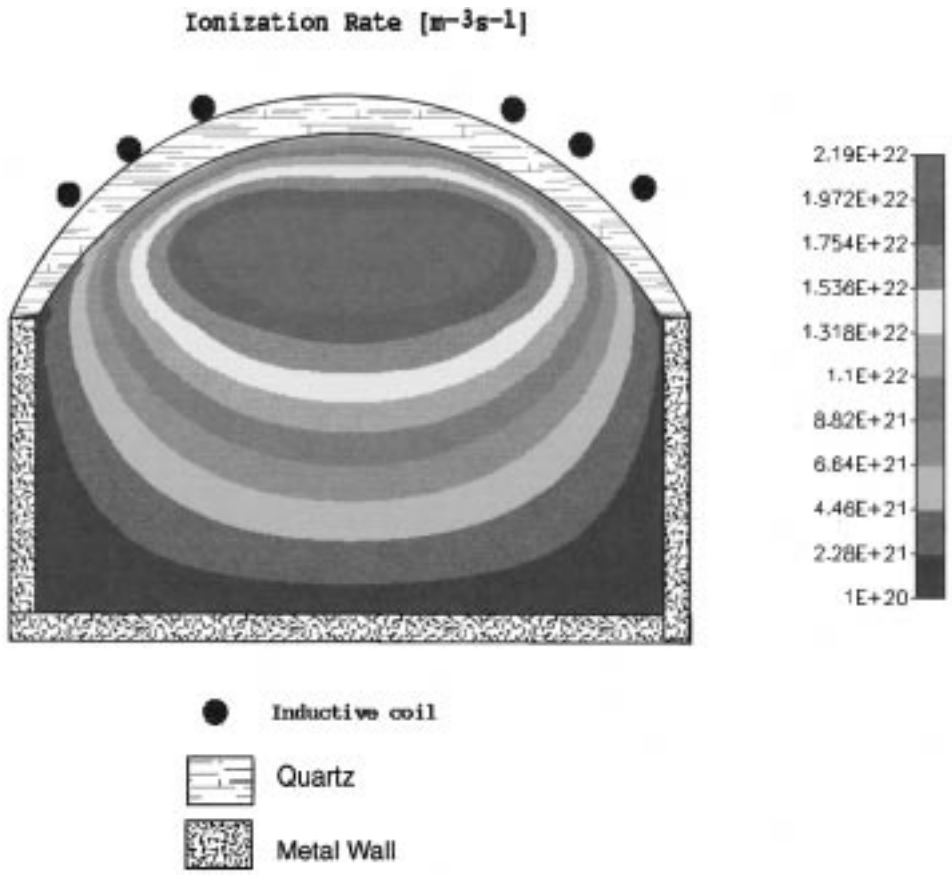

Fig. 7. Fluid model simulation result and spatial profile of the ionization rate $R_{\mathrm{ion}z}$, where $P_{\mathrm{abs}} = 200$ W, and $p_n = 10$ mtorr.

The equations for E_1 and E_2 are

$$\nabla^2 E_1 - \frac{E_1}{r^2} + \left(\frac{\omega^2}{c^2} - \frac{\xi\omega^2\sigma_c}{\nu_{en}}\right)E_1 - \xi\sigma_c\omega E_2 = 0 \quad (12)$$

$$\nabla^2 E_2 - \frac{E_2}{r^2} + \left(\frac{\omega^2}{c^2} - \frac{\xi\omega^2\sigma_c}{\nu_{en}}\right)E_2 + \xi\sigma_c\omega E_1 = 0 \quad (13)$$

where $\xi = 4\pi\times10^{-7}$ H/m, ν_{eN} is the electron-neutral collision frequency, and $c = 3 \times 10^8$ m/s is the speed of light. The boundary condition for (12)–(13) are $E = 0$ on the metallic wall and the axis. The boundary condition on the quartz bell jar is determined by the coil current $I = I_0 \cos \omega t$. The detailed deductive expression can be found in [8].

C. Theoretical Results

1) Global Model Results: If N and d_{eff} are known, (3) can be solved. For the ICP in this study (see Fig. 1), neutral gas pressure $p_n = 1$ mtorr, $P_{\mathrm{abs}} = 200$ W, and $\sigma = 0.8 \times 10^{-18}$ m^2, $N = 1.38 \times 10^{19}$ m^{-3}.

$$u_B = 1546\sqrt{T_e}$$
$$\lambda_i = \frac{1}{N\sigma} = 0.07 \text{ m}$$
$$h_L = 0.455$$
$$h_R = 0.335$$
$$d_{\mathrm{eff}} = 0.075.$$

Therefore, $T_e = 6$ eV with the K_{iz} value taken from (1) with $E_i = 15.75$ eV. Meanwhile, one can obtain the ion impacting energy, i.e., the ion hitting wafer with energy of $\varepsilon_i = 5.2T_e = 31.2$ eV. In addition, one can get the maximum plasma density

$$n = 0.62 \times 10^{17}/\mathrm{m}^3$$

and

$$J_b = h_L n u_B = 1.76 \text{ mA/cm}^2$$

by solving (7).

The relation of T_e versus p_n, i.e., the solution of (3), is displayed in Fig. 2, where the total power input is 200 W. It is found that the electron temperature is relatively insensitive to neutral gas pressure. As the gas density decreases, the ionization rate coefficient must increase to keep the balance of ion creation and loss rates. The dependence of plasma density on neutral gas pressure is shown in Fig. 3.

2) Fluid Model Results: Fig. 4 shows the power deposition profile with 10 mtorr neutral gas pressure and a 200-W power input. It is found that much of the power is absorbed on the top side area. Fig. 5 shows the electron temperature distribution. As in the previous result with the cylindrical chamber, T_e is quite uniform in the bulk plasma. The difference between the maximum on the upper centerline and the minimum at the bottom is less than 1 eV. With this relatively flat temperature profile, the spatial profiles of the plasma density and ionization rate are quite similar. Fig. 6 is the spatial profile of the electron density. The maximum can exceed 10^{11}/cm^3. The plasma density contours show that the density uniformity is fairly good

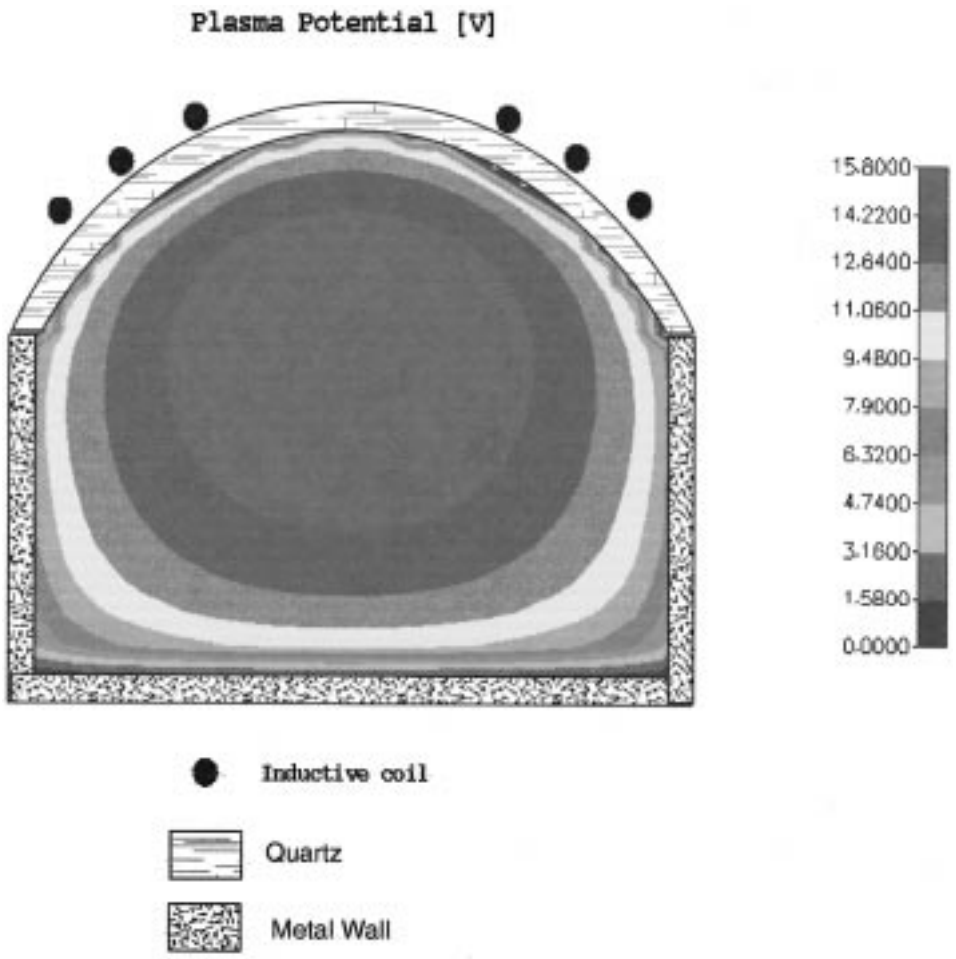

Fig. 8. Fluid model simulation result and spatial profile of the plasma potential ϕ, where $P_{\rm abs} = 200$ W, and $p_n = 10$ mtorr.

in the near bottom area. The ionization rate is similar to the electron density distribution (see Fig. 7). The plasma potential is shown in Fig. 8, where the maximum is about 15 V. This low potential leaves room to use bias to independently control the ion-impacting energy.

III. Experimental Diagnosis

A. Description of the Measurements

The experimental apparatus is operated with a 13.56-MHz power supply. The forward and reflected power is manually adjusted to ensure that the reflection is less than 5%. The operational power input varies from 100–600 W. The pressure can be set from 1–50 mtorr and is measured by a pressure gauge. The discharge chamber is grounded and pumped by a turbomolecular pump capable of attaining a base pressure of less than 10^{-6} Pa. The flow of gases is controlled by an MKS flow controller.

Due to serious RF interference, a conventional probe characteristic usually overestimates the electron temperature and underestimates the electron density. Some double probes have been reported for RF plasma diagnostics [18]. In the present study, a tuned probe had to be used to minimize the RF voltage across the sheath during the diagnosis. The tuned Langmuir probe technique is based on the concept that a passive circuit

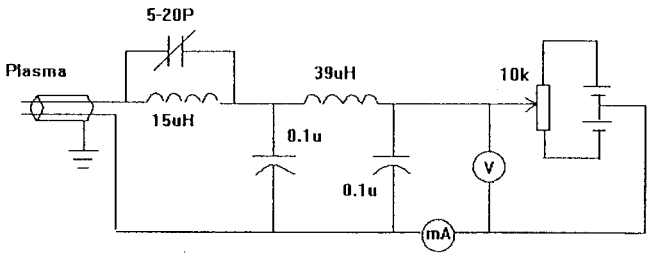

Fig. 9. Sketch of the experimental arrangement circuit for the tuned Langmuir probe.

makes the probe behave as if it were connected to a high-impedance circuit. In contrast to the driven probe technique, it requires significantly less hardware to implement. The detailed technique can be found in [13] and [15]. Fig. 9 is a sketch of the experimental arrangement circuit for the tuned Langmuir double probes. The filter networks reduce the RF voltage to less than millivolt levels.

The chamber is equipped with a special port through which the Langmuir probe is inserted into the bulk plasma. Using the double probes, plasma parameters, such as plasma density n and electron temperature T_e, have been measured. The observation points are at $z = 3, 6, 9$, and 12 cm and $r = 0, 2.5, 5$, and 7.5 cm, respectively. The probe can be rotated a

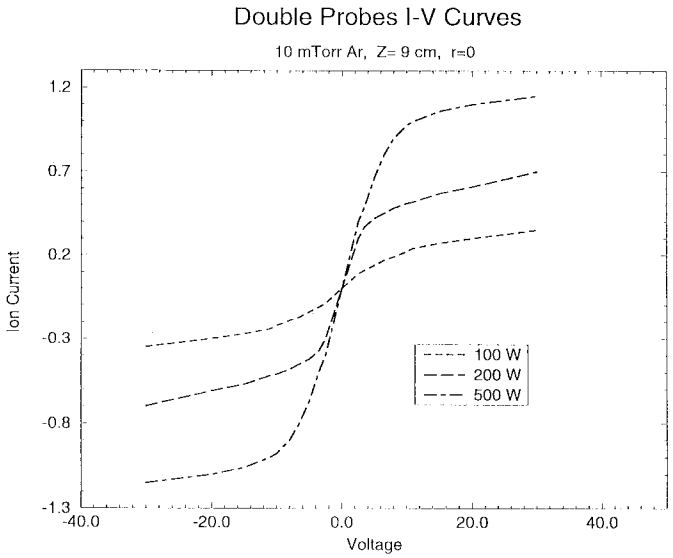

Fig. 10. Double-probe I–V curves with respect to $P_n = 10$ mtorr, $P_{\rm abs} = 100, 200,$ and 500 W, respectively.

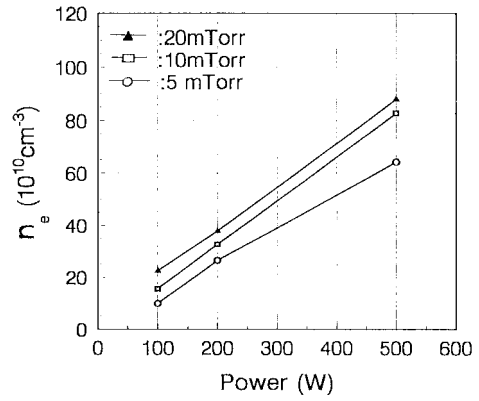

Fig. 11. Electron densities versus power inputs $P_n = 5, 10,$ and 20 mtorr, respectively. The observation position is at $z = 9$ cm, and $r = 0$.

certain angle to measure different radial points. On the wafer stage, RF bias can be applied to wafer with a frequency of 100 kHz. The total bias power input is limited by the RF supply (less than 50 W).

B. Experimental Results

Measurements were made over a neutral gas pressure range of 5–20 mtorr. The probe tips are 0.8 mm in diameter. The probe light versus current (I–V) curves are obtained by an oscilloscope with a memory. The plasma bulk parameters seem independent of the RF bias.

1) Plasma Density: Fig. 10 shows the I–V curves for different values of the RF power input. Time averaging is done to smooth the oscillations. Fig. 11 shows the relationship between electron densities and power inputs for different neutral pressures. It verifies the linear relationship between the plasma density and power input, i.e., lower neutral pressures result in lower plasma densities. This trend is the same as the global model prediction.

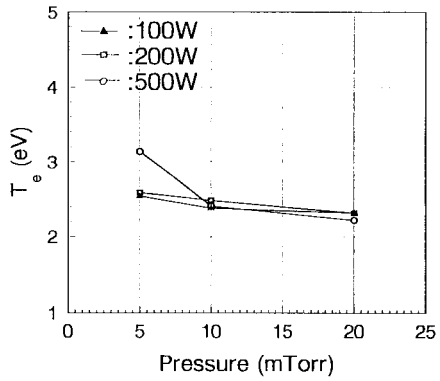

Fig. 12. Electron temperature T_e versus neutral pressure p_n, power input $P_{\rm abs} = 100, 200,$ and 500 W, respectively.

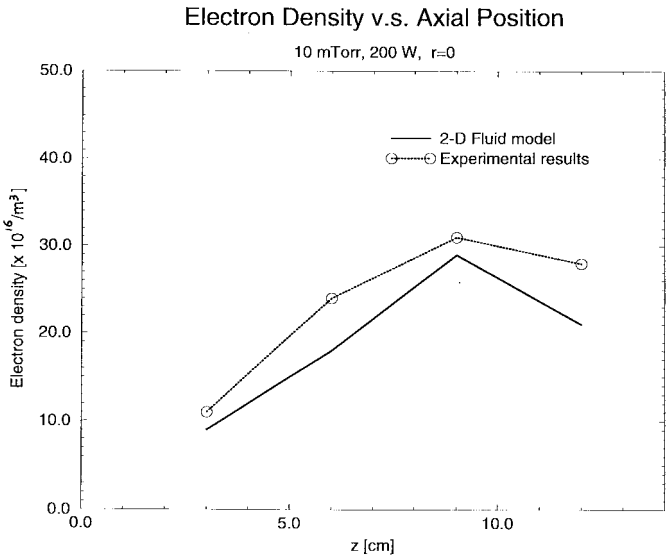

Fig. 13. Spatial comparison of the electron densities on the Z axis, where $P_{\rm abs} = 200$ W, and $P_n = 10$ mtorr.

2) Electron Temperature: Fig. 12 shows the measured value of the electron temperature at the points $r = 0$ and $z = 9$ cm. It shows that the electron temperature is not as sensitive to both gas pressure and power input in the pressure range of 10–20 mtorr. However, as the pressure goes down further, more power input is needed to raise the electron temperature. At very low pressures, T_e must be raised to make the ionization rate large enough to keep the balance of ion creation and loss.

IV. Conclusion and Discussion

The predictions of a global model and a 2-D fluid model were compared with measurements on a bell-bar-top ICP reactor. Figs. 2–3 show the comparisons for electron temperature and electron density, respectively. The differences among these depend primarily on how the spatial average was taken and where the data were measured. The following results show the comparisons of spatial distributions predicted by the 2-D model and those measured in the experiments. Although there

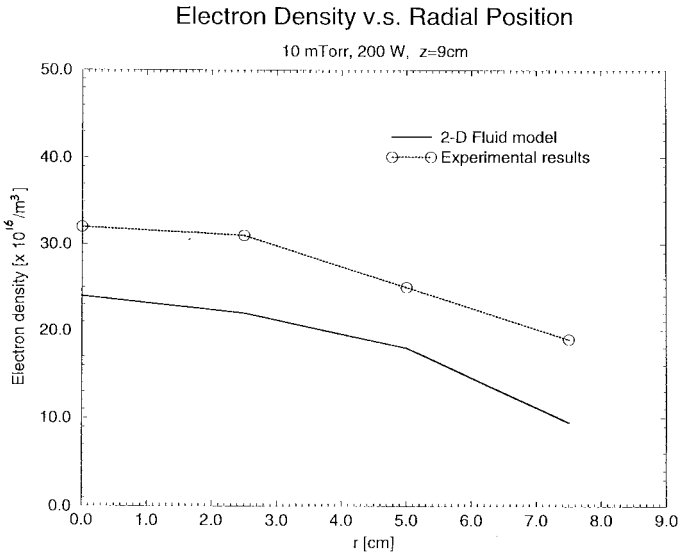

Fig. 14. Spatial comparison of the electron densities on the radial direction, where $P_{\rm abs} = 200$ W, and $P_n = 10$ mtorr.

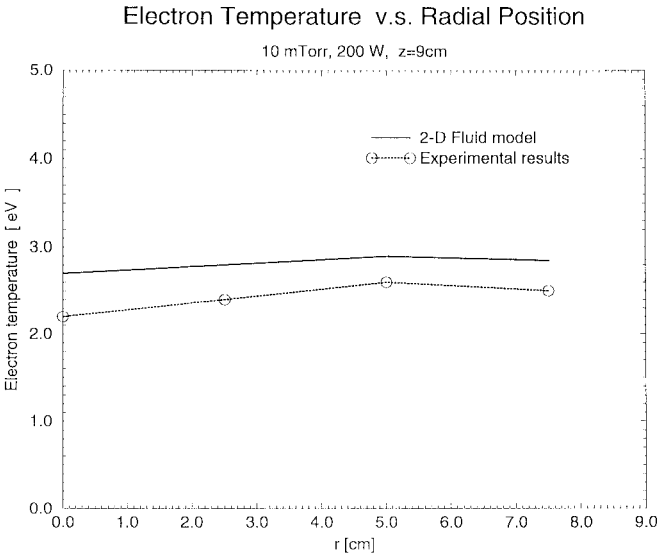

Fig. 16. Spatial comparison of the electron temperatures on the radial direction, where $P_{\rm abs} = 200$ W, and $P_n = 10$ mtorr.

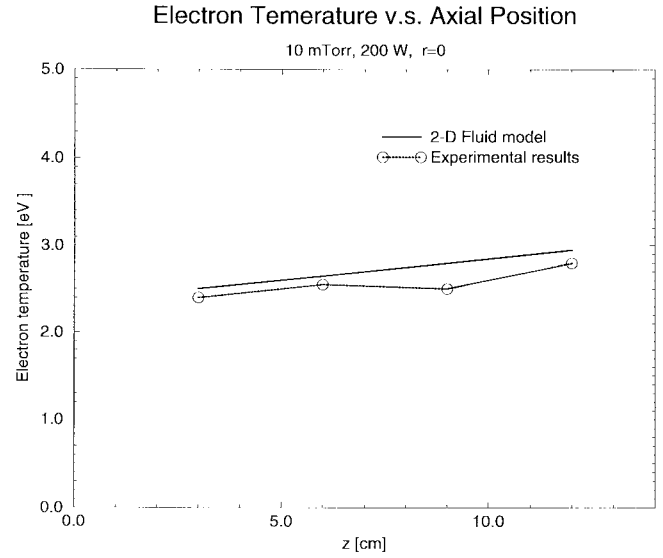

Fig. 15. Spatial comparison of the electron temperatures on the Z axis, where $P_{\rm abs} = 200$ W, and $P_n = 10$ mtorr.

are no error bars for experimental presentations in the figures, the relative error has been estimated in the range of $\pm 5\%$.

Figs. 13 and 14 are the spatial distribution comparisons for the electron densities on the Z axis ($r = 0$) and in the radial direction ($z = 9$ cm), respectively. The neutral pressure is 10 mtorr and the power input is 200 W. From Figs. 13 and 14, it is found that the model predictions are in good agreement with the data. The simulation predicts a lower density compared to the experimental measurement. One reason for this could be the fact that only ohmic heat was considered in the model. The collisionless heating may be significant. This is primarily a kinetic effect, but nonetheless may be incorporated in the fluid model [19].

Figs. 15 and 16 show the spatial distribution comparisons for the electron temperature on the Z axis ($r = 0$) and in the radial direction ($z = 9$ cm), respectively. It is observed that the electron temperature is quite uniform in the plasma bulk. The strong electron thermal conductivity transports the energy effectively to reduce the gradient in the electron temperature. The figures also show that the model predictions of electron temperature are higher than the measured values. Due to the limitation of double probes, the measured electron temperatures in Figs. 15 and 16 should be lower than their actual values. Consideration of this factor will bring the simulations in closer agreement with data.

ACKNOWLEDGMENT

The authors gratefully acknowledge Prof. D. B. Graves for his comments on the paper.

REFERENCES

[1] M. A. Lieberman and R. A. Gottscho, "Design of high density plasma source for material processing," in *Physics of Thin Films*, M. Francombe and J. Vossen, Eds. Orlando, FL: Academic, 1994.
[2] M. A. Lieberman and A. J. Lichtenberg, *Principles of Plasma Discharges and Materials Processing.* New York: Wiley-Interscience, 1994.
[3] D. B. Graves, "Plasma processing," *IEEE Trans. Plasma Sci.*, vol. 22, p. 31, 1994.
[4] H.-M. Wu, D. W. Dong, and J. Y. Xu, "Comparison between ICP and ECR plasma reactors" (in Chinese), *Mater. Electron.*, vol. 12, p. 7, 1994.
[5] R. Stewart, P. Vitello, and D. B. Graves, "2-D fluid simulation of high density inductively coupled plasma sources," *J. Vac. Sci. Technol. B*, vol. 12, p. 478, 1994.
[6] J. H. Keller, J. C. Forster, and M. S. Barnes, "Novel rf induction plasma processing techniques," *J. Vac. Sci. Technol. A*, vol. 11, p. 2487, 1993.
[7] J. Hopwood, "Ion bombardment energy distribution in rf induction plasma," *Appl. Phys. Lett.*, vol. 62, p. 940, 1993.
[8] M. Li, H.-M. Wu, and Y.-M. Chen, "2-D simulation of inductive plasma sources with self-consistent power deposition," *IEEE Trans. Plasma Sci.*, vol. 23, p. 558, 1995.
[9] H.-M. Wu, M. Li, and Y.-M. Chen, "Global model estimation for bell jar ICP parameters," *Chin. Phys. Lett.*, vol. 12, no. 5, p. 281, 1995.
[10] P. L. Ventzek, R. J. Hochstra, and M. J. Kushner, "2-D modeling of high plasma density inductively sources for material processing," *J. Vac. Sci. Technol. B*, vol. 12, p. 25, 1994.
[11] R. K. Porteous, H.-M. Wu, and D. B. Graves, "A two-dimensional axisymmetric model of magnetized glow discharge plasma," *Plasma Sources Sci. Technol.*, p. 25, 1994.

[12] H.-M. Wu, D. B. Graves, and R. K. Porteous, "Comparison between a 2-D simulation and a global conservation model for a compact ECR plasma source," *Plasma Sources Sci. Technol.*, p. 4, 1995, p. 22, 1995.
[13] C. Lai, R. A. Breun, P. W. Sandstrom, A. E. Wendt, and N. Hershkowitz, "Langmuir probe measurements of electron temperature and density scaling in multidipole radio frequency plasma," *J. Vac. Sci. Technol. A*, vol. 11, no. 4, p. 1199, 1993.
[14] L. Mahoney, A. E. Wendt, E. Barrios, and C. J. Richards, "Electron-density and energy distributions in a planar inductively coupled discharge," *Appl. Phys.*, vol. 76, no. 4, p. 2041, 1994.
[15] A. P. Paranjpa, J. P. McVittie, and S. A. Self, "A tuned Langmuir probe for measurements in RF glow discharges," *J. Appl. Phys.*, vol. 67, no. 11, p. 6718, 1990.
[16] V. I. Kolobov, D. F. Beale, L. J. Mahoney, and A. E. Wendt, "Nonlocal electron kinetics in a low-pressure inductively coupled radio-frequency discharge," *Appl. Phys. Lett.*, vol. 65, no. 5, p. 537, 1994.
[17] U. Kortshagoen and L. D. Tsendin, "Fast two-dimensional self-consistent kinetic modeling of low-pressure inductively coupled RF discharge," *Appl. Phys. Lett.*, vol. 65, no. 11, p. 1355, 1994.
[18] B. M. Annaratone, G. F. Counsell, H. Kawano, and J. E. Allen, "On the use of double probes in RF discharges," *Plasma Sources Sci. Technol.*, no. 1, p. 232, 1992.
[19] V. Vahedi, M. A. Lieberman, G. DiPeso, T. D. Rognlien, and D. Hewett, "Analytic model of power deposition in inductively coupled plasma sources," *J. Appl. Phys.*, vol. 78, no. 3, p. 1446, Aug. 1995.

Han-Ming Wu was born in Shanghai, China. He received the Ph.D. degree from the Institute of Mechanics, Chinese Academy of Sciences, Beijing, in 1987.

He is a Senior Engineer with CFD Research Corporation, Huntsville, AL, and is currently performing a research project on high-density plasma reactors for the semiconductor industry. He has been interested in plasma-assisted material processing research work, such as ECR and ICP research, both in the theoretical and experimental areas.

Ben W. Yu was born in Hunan, China, in 1957. He received the B.S. degree from Huazhong University of Science and Technology, Wuhan, China, in 1982 and the M.S. and Ph.D. degrees in mechanical engineering from the University of Minnesota, Minneapolis, in 1989 and 1994, respectively.

Since he joined CFD Research Corporation, Huntsville, AL, in 1994, he has been the Principal Investigator on DARPA-funded research projects such as materials processing plasma, plasma equipment modeling, and particle contaminants in plasmas. His research work has included chemical vapor deposition of diamond thin films and thermal plasmas.

Anantha Krishnan received the Ph.D. degree from the Massachusetts Institute of Technology, Cambridge, in 1989.

His research focused on the development of computational techniques to simulate the turbulent transport of heat, mass, and momentum in unsteady reacting flows. At CFD Research Corporation, Huntsville, AL, he has been actively engaged in developing models for materials processing techniques such as chemical vapor deposition (CVD). He has had extensive experience in modeling transport processes in multicomponent media with homogeneous and heterogeneous chemical reactions including plasma enhancements. He is currently working with DARPA and SEMATECH to develop integrated virtual prototyping tools for semiconductor fabrication equipment. He is the author of more than 30 publications in international journals.

Ming Li was born in Henan, China, in 1967. He received the B.S. degree from Beijing University of Aeronautics and Astronautics, and the M.S. degree in fluid dynamics from the Institute of Mechanics, Chinese Academy of Sciences, Beijing, China, in 1988 and 1991, respectively.

Since he joined the Plasma Division of the Institute of Mechanics in 1991, he has engaged in numerical simulations of plasma and the study of particle–plasma interaction. In February 1995, he joined the Department of Chemical Engineering, University of California at Berkeley, as a Visiting Researcher, and he is now performing research on high-density plasma models and simulations.

Yun Yang was born in Hunan, China, in 1966. He received the B.S. degree in physics from Yunnan University, Kunming, China, in 1986 and the M.S. and Ph.D. degrees in material physics from Beijing Science and Technology University, China, in 1989 and 1994, respectively.

He joined the Plasma Division of the Institute of Mechanics, Chinese Academy of Sciences, Beijing, in 1994. His research interests include plasma-assisted materials processing, modeling plasma processing equipment, and other related topics in semiconductor etching.

Jia-Ping Yan is a Senior Engineer with the Institute of Mechanics, Chinese Academy of Sciences, Beijing.

Ding-Pu Yuan is a Research Professor with the Institute of Physics, Chinese Academy of Sciences, Beijing.